LUND UNIVERSITY

Denoising of arterial spin labeling data: wavelet-domain filtering compared with Gaussian smoothing.

Bibic, Adnan; Knutsson, Linda; Ståhlberg, Freddy; Wirestam, Ronnie

Published in:
Magma

DOI:
10.1007/s10334-010-0209-8

2010

Link to publication

Citation for published version (APA):
Bibic, A., Knutsson, L., Ståhlberg, F., & Wirestam, R. (2010). Denoising of arterial spin labeling data: wavelet-domain filtering compared with Gaussian smoothing. *Magma*, *23*(3), 125-137. https://doi.org/10.1007/s10334-010-0209-8

Total number of authors:
4

General rights
Unless other specific re-use rights are stated the following general rights apply:
Copyright and moral rights for the publications made accessible in the public portal are retained by the authors and/or other copyright owners and it is a condition of accessing publications that users recognise and abide by the legal requirements associated with these rights.
- Users may download and print one copy of any publication from the public portal for the purpose of private study or research.
- You may not further distribute the material or use it for any profit-making activity or commercial gain
- You may freely distribute the URL identifying the publication in the public portal

Read more about Creative commons licenses: https://creativecommons.org/licenses/

Take down policy
If you believe that this document breaches copyright please contact us providing details, and we will remove access to the work immediately and investigate your claim.

LUND UNIVERSITY

PO Box 117
221 00 Lund
+46 46-222 00 00

Download date: 19. Dec. 2025

LUND UNIVERSITY
Faculty of Medicine

LUP
Lund University Publications
Institutional Repository of Lund University

This is an author produced version of a paper published in Magma (New York, N.Y.). This paper has been peer-reviewed but does not include the final publisher proof-corrections or journal pagination.

Citation for the published paper:
Adnan Bibic, Linda Knutsson, Freddy Ståhlberg, Ronnie Wirestam

"Denoising of arterial spin labeling data: wavelet-domain filtering compared with Gaussian smoothing."

Magma (New York, N.Y.) 2010 May 4

http://dx.doi.org/10.1007/s10334-010-0209-8

Access to the published version may require journal subscription.
Published with permission from: Springer

Denoising of arterial spin labelling data: Wavelet-domain filtering compared with Gaussian smoothing

Authors: Adnan Bibic[1], Linda Knutsson[1], Freddy Ståhlberg[1,2], Ronnie Wirestam[1]

Communicating author: Adnan Bibic;
e-mail: adnan.bibic@med.lu.se
Telephone: +46 46 17 85 46
Fax: +46 46 17 85 40

Word count of abstract: 199

Word count of text: 6337

Number of figures and tables: 10

Number of references: 27

---

[1] Department of Medical Radiation Physics, Lund University, Lund, Sweden
[2] Department of Diagnostic Radiology, Lund University, Lund, Sweden

ABSTRACT

Purpose: To investigate a wavelet-based filtering scheme for denoising of arterial spin labelling (ASL) data, potentially enabling reduction of the required number of averages and the acquisition time.

Methods: ASL magnetic resonance imaging (MRI) provides quantitative perfusion maps by using arterial water as an endogenous tracer. The signal difference between a labelled image, where inflowing arterial spins are inverted, and a control image is proportional to blood perfusion. ASL perfusion maps suffer from low SNR and the experiment must be repeated a number of times (typically more than 40) to achieve adequate image quality. In this study, systematic errors introduced by the proposed wavelet-domain filtering approach were investigated in simulated and experimental image datasets and compared with conventional Gaussian smoothing.

Results: Application of the proposed method enabled a reduction of the number of averages and the acquisition time by at least 50% with retained standard deviation, but with effects on absolute CBF values close to borders and edges.

Conclusions: When the ASL perfusion maps showed moderate to high SNRs, wavelet-domain filtering was superior to Gaussian smoothing in the vicinity of borders between grey and white matter while Gaussian smoothing was a better choice for larger homogeneous areas, irrespective of SNR.

Key words: magnetic resonance imaging; arterial spin labelling; cerebral blood flow; perfusion; wavelets; filtering; denoising

INTRODUCTION

Arterial spin labelling (ASL) MRI has attracted considerable attention during recent years, not only for the potential to quantify perfusion in absolute terms [1] but also for being completely non-invasive. In some cases, for example, in neonates and even foetuses, ASL is one of few ethically justifiable options for perfusion studies [2]. The ASL technique employs arterial water as an endogenous freely diffusible tracer. The longitudinal magnetization of the inflowing water spin population is inverted, proximal to the imaging slice, typically by a *180°* radio frequency (RF) pulse, and magnetically labelled water arrives to the region of interest and contributes to a reduction of the local longitudinal magnetization and subsequently to a slight decrease of the signal in the acquired MR images. The degree of signal reduction is directly related to the local perfusion or regional cerebral blood flow (CBF). The ASL perfusion maps are constructed by subtraction of a tagged or labelled image from a control image (obtained by an experiment without inversion of inflowing spins), and the intensity of the difference image is directly proportional to blood perfusion. The ASL technique has previously been described in a number of publications [1,3-6].

The signal-to-noise ratio (SNR) is a critical issue in ASL techniques, especially in techniques aimed at absolute CBF quantification, such as QUIPSS [4] and Q2TIPS [7], in which a part of the labelled water is saturated to make the sequence insensitive of transit delay and for better estimation of the tag width (τ) of the tracer. In order to obtain an adequate image quality, averaging of a number of ASL images (typically of the order of 40-100 images) is required [7-10], leading to fairly long acquisition times. Higher image SNR would reduce the required number of averages, and approaches to achieve this are, for example, to directly increase the signal by increasing the magnetic field strength, improving the efficiency of receiver coils or exploring alternative pulse sequences and ASL techniques with improved SNR [11]. Another potential approach to reduce the number of averages is to employ a denoising algorithm by appropriate post-processing. The idea of applying spatial filtering to MR images is not new. For example, Gaussian smoothing is recommended as a preprocessing step in ASL-fMRI analysis in order to obtain acceptable statistical inferences [12] and a variety of wavelet-based denoising methods has been proposed for filtering of MR images; Alexander et al. [13] achieved an improvement in SNR and contrast in morphological MR images by denoising the real and imaginary parts of the signal separately, Nowak [14] presented a wavelet-domain filtering algorithm that effectively removed Rician noise at low SNR from the squared magnitude images, Wirestam et al. [15] applied wavelet-domain filtering for noise reduction of diffusion-weighted images in order to reduce the rectified noise floor at high b-values and Zaroubi and Goelman [16] successfully applied wavelet filtering to blood oxygenation level dependent functional MRI (BOLD-fMRI). Wink and Roerdink [17] carried out a comprehensive comparison between wavelet-based denoising methods and conventional Gaussian smoothing, applied to BOLD-fMRI images.

Studies examining the possibilities and limitations of filtering of ASL images are, however, sparse despite the fact that low SNR is a well-documented problem. Furthermore, the fact that ASL data originate from the subtraction of two magnitude images (each following a Rician noise distribution), resulting in a difference map with a symmetric noise distribution that can be assumed to be Gaussian [17], makes ASL data well suited for the application of noise-reduction approaches that assume white noise. Hence, in the present study, the effects of a wavelet-domain filtering method on ASL images were investigated and compared to the more traditional Gaussian smoothing technique. The filtering methods were applied to simulated images with a known noise distribution as well as to experimental images with different noise levels.

THEORY

Brief overview of the discrete wavelet transform and multiresolution analysis

Analogous to Fourier series analysis, where a signal is decomposed into its independent Fourier modes with sinusoidals as the basis function, orthogonal wavelet analysis is the decomposition of the signal into its independent wavelet modes using an orthonormal family of basis functions. This is accomplished by convolving the given function (input vector, **X**) with translated and dilated wavelet and scaling functions. Orthogonal wavelet basis functions are recommended in the present context, because they preserve a Gaussian noise distribution.

A wavelet function $\psi(u)$, where $u \in (-\infty, \infty)$, has to satisfy two basic properties:

1. The integral of the function must be zero:

$$\int_{-\infty}^{\infty} \psi(u) du = 0 \qquad [1]$$

2. The integral of the square of the function must be unity:

$$\int_{-\infty}^{\infty} \psi^2(u) du = 1 \qquad [2]$$

Equation [1] is consistent with the function appearing as a wave, because function values above zero must be cancelled out by function values below zero, while Eq. [2] implies finite amplitude and a finite extension over *u*. These two properties lead to a function that looks like a “small wave”, thus the notation wavelet.

The discrete wavelet transform (DWT) transforms the input image, *x*, of $N \times N$ size, containing *N* number input series, {X$_1$, X$_2$, …, X$_N$} into discrete wavelet coefficients, *w*, and scaling coefficients, *s*, by the application of a so-called pyramid algorithm to accomplish multiresolution analysis [18].

A discrete wavelet filter, ψ, must satisfy Eqs. [1] and [2] but the integral is replaced by a summation and, in order to fulfil the orthonormality condition, the wavelet filter must satisfy Eq. [3] as well:

$$\sum_{k=0}^{K-1} \psi_k \psi_{k+2n} = \sum_{k=-\infty}^{\infty} \psi_k \psi_{k+2n} = \begin{cases} 1, & \text{if } n = 0 \\ 0, & \text{if } n \text{ is non-zero integer} \end{cases} \qquad [3]$$

K is an even integer giving the width of the filter, i.e. the number of coefficients in the filter vector, ψ.

The low-pass scaling filter, φ, is defined as the ‘quadrature mirror’ of the wavelet filter:

$$\varphi_k \equiv (-1)^{k+1} \psi_{K+1-k} \qquad [4]$$

The scaling coefficients ($s_{j_0,t}$) and the wavelet coefficients ($w_{j,t}$) are calculated by a circular convolution of the input image with the wavelet and low-pass scaling filters, respectively:

$$w_{j,t} \equiv \sum_{k=0}^{K-1} \psi_k V_{j-1,\, 2t+1-k \bmod N/2^{j-1}}, t = 0, \ldots, \frac{N}{2^j} - 1 \qquad [5]$$

$$s_{j,t} \equiv \sum_{k=0}^{K-1} \varphi_k V_{j-1,\, 2t+1-k \bmod N/2^{j-1}}, t = 0, \ldots, \frac{N}{2^j} - 1 \qquad [6]$$

where j is the wavelet scale or frequency band (with *j=1,…,J)*. The sample size N is equal to 2^J and V_0 is defined to be **X**. By transforming the input signal **X** (V_0) of length N into the N/2 first level wavelet coefficients w_1, and the N/2 first level scaling coefficients s_1, the first step of the pyramid algorithm for computing the DWT is completed. To finalize the pyramid algorithm there are J-1 subsequent steps j=2,…,J and at each step only the scaling coefficients s_{j-1} of length N/2^{j-1} are transformed into w_j and s_j of length N/2^j. At the end of the Jth step, the DWT output coefficient vector can be constructed by concatenating the coefficients w_1,…, w_J and s_J. This is performed for each row in the image matrix, x, and finally the matrix is rotated 90 degrees and the procedure is repeated.

For further information about the wavelet transform, the reader is referred to, for example, the textbook by Percival et al. [19].

MATERIALS AND METHODS

Simulated data

In order to include partial-volume effects close to borders between different types of tissue, synthetic image sets were constructed from T1-weighted morphological images with very high resolution ($0.83 \times 0.83 \times 0.90\ mm^3$) obtained using a magnetized prepared rapid gradient echo (MPRAGE) sequence, acquired with a 3T Philips Achieva MRI unit (Philips Medical Systems, Best, The Netherlands) using TR/TE=6.7/3.1 ms and flip angle *8º*. White-matter (WM) and grey-matter (GM) regions were segmented using the software package *Statistical Parametric Mapping v*.5, (SPM5, Wellcome Department of Imaging Neuroscience, London, UK; www.fil.ion.ucl.ac.uk/spm) executed in Matlab 7.3 (Mathworks, Sherborn, Massachusetts). White-matter pixels were assigned a CBF value of *25 ml/100g/min* while GM pixels were set to a CBF value of *65 ml/100g/min* corresponding to PET values reported for the normal human brain [23] (Figure 1). The images were subsequently down-sampled to $3.75 \times 3.75 \times 6.3\ mm^3$ (low-resolution image set) to correspond to a realistic ASL case, as well as to $1.875 \times 1.875 \times 3.6\ mm^3$ (high-resolution image set) to investigate future possibilities of using high-resolved ASL images. Since the noise in ASL perfusion maps (i.e. in difference images) can be assumed to follow a Gaussian distribution [20,24,25], different amounts of Gaussian noise were added to allow comparisons between different SNR levels (defined as the ratio of the mean signal value within the entire object region under investigation to the noise standard deviation corrupting the signal). In the simulated ASL perfusion maps, SNRs were set to integers between 1 and 12, and different SNR levels correspond to different numbers of averages in realistic ASL studies.

Experimental data

Experimental ASL images, obtained in three healthy volunteers, were acquired using a 3T MRI unit (Magnetom Allegra, Siemens AG, Erlangen, Germany) using the PICORE Q2TIPS pulse sequence [7], provided by the manufacturer. The imaging parameters were as follows: $TI_1/TI_{1s}/TI_2$=700/1300/1400 ms, TE/TR=15/2500 ms, FOV=240 mm, slice thickness = 7 mm, 10 cm inversion slab, 1 cm gap and a gradient-echo echo-planar imaging (GRE-EPI) readout acquisition with 64^2 matrix size. For volunteer #1, 300 difference images were acquired, while 40 difference images were obtained for volunteers #2 and #3. The experimental data from volunteer #1 were used to construct image sets with three different SNR levels by averaging 5, 20 or 45 randomly selected difference images, according to the *bootstrap* technique [27]. All three resulting image sets thus contained 1000 averaged difference images, each image showing SNR levels of approximately 4, 8 and 12, respectively, defined as the ratio of the mean signal value within the entire object to the standard deviation in a ROI placed within an artefact-free region of background outside the object. The entire procedure was repeated 100 times, i.e. 100 sets of 1000 averaged difference maps were constructed, to allow for statistical evaluation of the results (as described below). Image data from volunteers #2 and #3 were subject to the described denoising procedures, but were evaluated by visual inspection only.The examinations were approved by the local ethics committee and written informed consent was obtained from each volunteer prior to the study.

Denoising by Gaussian smoothing (GS)

Gaussian smoothing is a spatial filter which blurs the pixel values under a filter mask consisting of a Gaussian function. Mathematically, this operation constitutes a convolution of the image with the Gaussian function.

Denoising by wavelet-domain (WV) filtering

In the present study, noise reduction by Wiener-like filtering in the wavelet domain is proposed to allow a decrease in the number of averages and the acquisition time in ASL MRI. The filtering in the wavelet domain aimed at providing an approximation to the noise-free signal by appropriately modifying elements in the wavelet domain in such a way that noise components are removed while true signal is retained. The filtering was applied to the averaged difference images in which the noise can be assumed to be Gaussian distributed [20]. The basic filtering approach has been previously described [15], although presently modified to use a noise-variance assessment according to Alexander et al. [21].

The transformation of images from the spatial domain to the wavelet domain was accomplished by an orthogonal 2D DWT based on the routine described in section 13.10 of Ref. [22]. In the present report, the orthogonal wavelet-transform matrix is denoted W_i and the inverse wavelet transform W_i^{-1}, where the subscript *i* refers to the use of different wavelet bases coefficients. An overview of the filtering scheme is given in Figure 2. The averaged original image, *x*, represents the true object signal, *s*, degraded by a noise signal, *n*, (Eq. 7) which is assumed to be Gaussian as indicated above [20].

$$x = s + n \qquad [7]$$

After the discrete wavelet transform, W_1, of noisy data, *x*, the corresponding wavelet coefficients are obtained (Eq. 8).

$$y = \Theta_1 + z_1 \qquad [8]$$

where $y = W_1 x$, $\Theta_1 = W_1 s$ and $z_1 = W_1 n$. The first stage in the filtering scheme is a thresholding of coefficients in the wavelet domain, W_1, by a so-called hard threshold filter (denoted by the operator H_h) (Eq. 9), for which all coefficients are set to zero if the magnitude is below the threshold ρσ, and otherwise left unchanged (Eq.10). In this operation, ρ is an empirical threshold factor and σ is an approximation to the noise standard deviation (SD), given by the median absolute value of the finest scale wavelet coefficients, corrected by factor 1.4826 according to Alexander et al. [21].

$$H_h(i,j)=\begin{cases}1, & if\ |y(i,j)|\geq \rho\sigma \\ 0, & otherwise\end{cases} \qquad [9]$$

$$\hat{\theta}_1(i,j)=y_1(i,j)\cdot H_h(i,j) \qquad [10]$$

The distribution of noise z_1 in the wavelet domain remains unchanged since the use of an orthogonal wavelet implies that white noise is transformed into white noise, and the noise is uniformly distributed over all wavelet coefficients.

$$\hat{s}_1=W^{-1}H_hWx \qquad [11]$$

The estimated signal, $\hat{s}_1$, obtained by the inverse wavelet transform, W_1^{-1}, of filtered coefficients, (Eq. 11) is then used in the W_2 step to construct a Wiener-like filter (denoted H_W) (Eq. 12), from wavelet coefficients $\hat{\theta}_{21}(i,j)$ (Eq. 11).

$$H_w(i,j)=\frac{\left|\hat{\theta}_{21}(i,j)\right|^2}{\left|\hat{\theta}_{21}(i,j)\right|^2+\sigma^2} \qquad [12]$$

$$\hat{\Theta}_{21}=W_2\hat{s}_1 \qquad [13]$$

Subsequently, the Wiener-like filter was applied to $\hat{\theta}_{21}(i,j)$:

$$\hat{\Theta}_2=\hat{\Theta}_{21}\cdot H_w \qquad [14]$$

Finally, the estimated approximate signal, $\hat{s}_2=W_2^{-1}H_WW_2W_1^{-1}H_hW_1x$, obtained by the inverse wavelet transform W_2^{-1} is used to design a final Wiener-like filter (Eq. 15) in W_3 and this filter is applied to the original image data x in W_3.

$$\hat{H}_w(i,j)=\frac{\left|\hat{\theta}_{321}(i,j)\right|^2}{\left|\hat{\theta}_{321}(i,j)\right|^2+\sigma^2} \qquad [15]$$

The choice of wavelet family and wavelet order is also of importance, since different wavelet families and orders separate signal from noise in different manners. Hence, a mixture of different families and orders tends to give the best result, making it possible to reduce more noise after each step in the filtering process. In the present study, a viable combination was established by empirical tests, but it should be noted that the optimal wavelet combination is image and signal dependent and it is impossible to specify an ultimate combination of wavelet families and orders for a general case.

Post-processing and data analysis

The Gaussian smoothing was performed in SPM5 using two-dimensional smoothing kernels of FWHM=4 mm for the high-resolution simulated image set and 8 mm for the low-resolution simulated image set as well as for the experimental data. These smoothing kernels were selected to be approximately twice the in-plane image resolution, motivated by the fact that such a dimension reasonably well reflects the smallest lesion size that one would expect to target with the applied resolution. Furthermore, the matched filter theorem indicates that an optimal smoothing kernel should match the size of the signal-generating object to be detected [18].In addition, a smoothing kernel of FWHM=2.8 mm was applied to high-resolution simulated images and FWHM=5.6 mm to low-resolution simulated images and to experimental data as well, providing approximately equal variances in homogenous areas (in the middle of WM for low SNR images) after both smoothing and wavelet filtering.

Wavelet filtering was performed as described above using a locally developed computer program designed in Interactive Data Language (IDL 6.3, Research Systems Inc., Boulder, USA): $\mathbf{W_1}$ was the Haar wavelet, $\mathbf{W_2}$ was Daubechies of order 12 and $\mathbf{W_3}$ was Daubechies of order 5. The threshold factor in the hard-threshold filtering part was $\rho=2$.

Simulated data were used to investigate the usefulness of the filtering methods and to investigate potential systematic errors. In this analysis, the standard deviation from the true value (SDftv) was calculated in each pixel (x,y) for each repetition i of the N=1000 simulations carried out with different realizations of the noise. SDftv is defined as:

$$SDftv(x,y)=\sqrt{\frac{\sum_{i=1}^{N}\left(CBF_n(x,y)-CBF_{true}(x.y)\right)^2}{N}} \qquad [16]$$

The SDftv was employed, rather than the conventional SD from the mean value, since SDftv will include any systematic errors in the filtered images. Furthermore, a correspondingly modified coefficient of variation *CV* was calculated for each image set:

$$CV=\frac{SDftv(x,y)}{CBF_{true}(x,y)} \qquad [17]$$

The coefficient of variation provides a measure of the spread in data relative to the mean or, in our case, the true value. In order to evaluate the effects of filtering, the CVs before and after denoising and between the two filtering methods were compared by visualizing the CV difference (ΔCV):

$$\Delta CV = CV_A - CV_B, \qquad [18]$$

where A and B denote the different image sets in the comparison (noisy versus filtered, wavelet filtered versus Gaussian smoothed, etc.). ΔCV provides the amount of improvement or degeneration after filtering. To examine whether the observed ΔCV values were significantly different from zero, the procedure described above was repeated 100 times for each image set and a paired two-sample *t*-test (TM_TEST function in IDL), with multiple comparisons correction, was applied to the CV datasets. Pixels corresponding to a level of significance of $p \geq 1-0.95^{1/pn}$ (where pn is the number of pixels within the object) are shown in white in the ΔCV maps.

The bias introduced by the filtering methods, defined as the absolute value of the difference between the estimated mean value in a given pixel after filtering and the true value in that pixel, was calculated. The significance of the bias was assessed by an independent one-sample t-test with multiple comparisons correction ($p \leq 1-0.95^{1/pn}$).

The three image sets of experimental data, with different SNR levels, underwent similar image analysis as the simulated data, but in this case the result obtained using the maximal number of averages (300) was defined as the true (or reference) value $CBF_{true}(x,y)$.

Furthermore, the CBF and its standard deviation were calculated for selected pixels at different SNR levels using simulated and experimental data. Simulated data were analyzed before and after filtering in three selected areas depicted in Figure 1, i.e. in the middle of a region with homogenous CBF, in a region close to the border between grey and white matter and in the narrow region between two sulci. In experimental data, one pixel in the narrow region between two sulci (indicated in Figure 6a to the right) was investigated. Finally, to evaluate the improvement in SNR after wavelet-domain filtering, the mean SNR value in a region of interest (ROI) close to the border between GM and WM (Figure 1) was calculated before and after filtering.

RESULTS

The effects of different filtering methods on simulated ASL-based perfusion maps, evaluated by comparing the modified *CV* in each pixel before and after filtering as well as by comparing ΔCV between different filtering approaches, are summarized in Figure 3 and Figure 4: ΔCV for low- and high-resolution simulated images is displayed at SNR levels of 4, 8 and 12. Similar results for averaged experimental images (i.e. for SNR levels of 4, 8 and 12) are given in Figure 5 Pixels in blue in columns (a), (b) and (d) indicate locations where the filtering was superior to non-filtered images, while pixels in red show locations where the applied filtering method failed to improve the CBF result. A comparison between the two noise-reduction algorithms is given in columns (c) and (e), in which pixels in blue show the positions where the wavelet-domain filtering was superior and pixels in red indicate where Gaussian smoothing was superior. In columns (b) and (c) the applied smoothing kernel was FWHM=8 mm while in columns (d) and (e) the used smoothing kernel was FWHM=5.6 mm. The colour bars show the different levels of ΔCV, and pixels in white show locations where no significant mean difference between the *CV* populations was observed.

The visual appearance of images resulting from the two filtering methods is illustrated in Figure 6, showing images from experimental data after various degrees of averaging and

filtering. Figure 6a, column ii shows a non-averaged difference image from volunteer #1 (also illustrating an artefact in the sagittal-sinus region) and Figure 6a, column iii, displays the high-SNR image reconstructed from 300 difference images, serving as a reference image. Figure 6b (volunteer #1) illustrates (i) the low-SNR image that was reconstructed from 5 experimental difference images, (ii) the image filtered by the wavelet-domain noise-reduction algorithm, (iii) the Gaussian smoothed image (FWHM=8 mm) and (iv) the Gaussian smoothed image (FWHM=5.6 mm). Figures 6c, (volunteer #1), 6d (volunteer #2) and 6e (volunteer #3) show the corresponding information as in 6b but in these cases the images are reconstructed by averaging 20 difference images (SNR=8).
Figure 7 shows the means and standard deviations of CBF for pixels in (a-c) three different regions (according to Figure 1) in simulated images images and (d) for one pixel in experimental images (according to Figure 6a, column iii). Results were based on 1000 iterations with different realizations of the noise.

Figures 8 and 9 show maps of the bias caused by the filtering methods. Pixels showing no significant bias are displayed in black.

Figure 10 illustrates the mean relative filtering-induced improvement in SNR as a function of SNR for a pixel in WM after wavelet filtering as well as Gaussian smoothing with FWHM=8 mm (corresponding to pixel location 1 in Figure 1).

DISCUSSION

In the present study, the effects of wavelet filtering and Gaussian smoothing on the quality of simulated and experimental ASL perfusion maps were compared, and detailed analysis of pixels in selected regions within the object showed how the standard deviations and mean values of CBF were influenced by the filtering at different noise levels ($4 \leq SNR \leq 12$).

The results indicate that deviations from the true or reference value were significantly decreased by both filtering methods in almost the entire object, particularly at low SNR. Near tissue borders or edges, both wavelet-domain filtering and Gaussian smoothing failed to improve the result, presumably since both filtering methods induce some degree of spatial smoothing. However, the wavelet filtering generally retained the spatial resolution better than

Gaussian smoothing in edge areas, as well as in the vicinity of borders between grey and white matter, particularly in areas with somewhat higher SNR. This is highlighted in Figures 8 and 9, in which it is clearly indicated that the bias caused by wavelet filtering was considerably smaller than for Gaussian smoothing. For the experimental data, it should also be noted that the apparent superiority of Gaussian smoothing in the posterior region (close to the sagittal sinus) is a result of the artifact visualized in Figure 6a. Apart from this artefact, the trend is the same as for the simulated images but moderately subdued.

The wavelet-domain filtering method decreased the standard deviation and increased the accuracy of simulated values, especially for low-SNR data. With increasing SNR, the gain fades out and above approximately SNR=10 filtering contributes very little to the improvement of the results (Figure 10. Reduced noise potentially enables a more precise and accurate experimental estimation of the absolute CBF values. The noise reduction can also be used to reduce the number of averages, giving a correspondingly shorter acquisition time, or to increase the spatial resolution. As an example, assuming a typical SNR of approximately 15 in non-filtered ASL data obtained with 40 repetitions, our investigation indicates that a reduction from 40 to 27 averages could be achieved by the use of wavelet filtering with retained SNR. This corresponds to a reduction in acquisition time by at least 30%, and the gain would, obviously, be even larger for images suffering from lower SNR (Figure 9). Since many deconvolution algorithms are known to be sensitive to noise, filtering might be particularly useful in ASL applications requiring deconvolution, such as model-free ASL using QUASAR [26], provided that spatial filtering effects does not hamper accurate registration of the arterial input function. Reduction of the number of averages may also reduce the risk of patient movement and associated motion artifacts, but can, on the other hand, introduce more physiological noise in the data, for example, if the effects of cardiac pulsations, causing different amounts of blood being labelled from one image to the next, are not completely averaged out. Wu et al. [9] investigated the effects of cardiac pulsation in ASL and concluded that the CBF signal was significantly higher and the transit delay was shorter if blood was labelled during systole than during diastole in healthy volunteers.

The other investigated approach, Gaussian smoothing, is an effective filtering method that removes noise-induced fluctuations but, unfortunately, this improvement is typically accompanied by a well-known loss of object detail. In large, fairly homogeneous areas, the Gaussian smoothing is superior to most other filtering methods. In some applications, such as

ASL perfusion imaging, the image resolution is of the same order of magnitude as the size of the human sulcus, and information near edges and borders should preferably be preserved. Hence, a method which does not degenerate the signal in such areas is warranted. The wavelet filtering algorithm shows a potential to improve the image quality, with similar performance as Gaussian smoothing in homogeneous areas, but showing the additional advantage of causing limited influence on the signal in areas close to borders and edges, although the gain naturally becomes smaller with increased SNR. Images filtered by Gaussian smoothing showed large degeneration in border areas, independently of the SNR level, while the proposed wavelet-domain filtering method, being an adaptive denoising method, showed a reduction of the bias near borders at higher SNR. In this context, it is important to point out that the biased values and standard deviations seen after wavelet filtering remained within the original (non-filtered) standard deviations while this was not the case for Gaussian smoothing. Comparing the two methods, the wavelet denoising method is generally preferable over Gaussian smoothing for denoising of ASL images because the wavelet-domain filter adapts automatically to the noise distribution of the input image, while the Gaussian smoothing kernel, according to the matched filter theorem [18], must match the object size to be detected. Finally, motion artefacts often lead to an incomplete static tissue subtraction in the difference maps, and one major benefit of filtering ASL images might be the possibility to reduce motion artefacts in the data by minimizing the acquisition time.

CONCLUSION

In conclusion, the results from both simulations and experiments illustrate that wavelet-domain filtering might be used to increase SNR in ASL images, as well as to increase the visual quality. Both wavelet-domain filtering and Gaussian smoothing methods corrupted the signal in areas close to borders but for the wavelet-domain filter this effect decreased with higher SNR, while for Gaussian smoothing it remained the same independently of SNR. If time allows, optimal quality of ASL-based CBF maps is always best accomplished by extending the number of averages, provided that the subject does not undergo any movement during the image acquisition. Filtering is, however, an attractive way to maintain precision and accuracy with a reduced number of averages, with potential usefulness also in dynamic applications such as ASL-fMRI and model-free ASL techniques [26].

ACKNOWLEDGEMENTS

The authors wish to thank Markus Nilsson, MSc, for helpful input regarding the bootstrap technique and the choice of t-test analysis. This study was supported by the K&A Wallenberg foundation (grant no. 1998.0182), the Swedish Research Council (grants no. 13514, 2005-6910, 2007-3974 and 2007-6079), the Crafoord foundation, the Cancer Foundation and the Lund University Hospital Donation Funds.

REFERENCES

1. Buxton RB, Frank LR, Wong EC, Siewert B, Warach S and Edelman RR (1998) A general kinetic model for quantitative perfusion imaging with arterial spin labeling. Magn Reson Med 40: 383-96
2. Wang J, Licht DJ, Jahng GH, Liu CS, Rubin JT, Haselgrove J, Zimmerman RA and Detre JA (2003) Pediatric perfusion imaging using pulsed arterial spin labeling. J Magn Reson Imaging 18: 404-13
3. Detre JA, Zhang W, Roberts DA, Silva AC, Williams DS, Grandis DJ, Koretsky AP and Leigh JS (1994) Tissue specific perfusion imaging using arterial spin labeling. NMR Biomed 7: 75-82
4. Wong EC, Buxton RB and Frank LR (1998) Quantitative imaging of perfusion using a single subtraction (QUIPSS and QUIPSS II). Magn Reson Med 39: 702-8
5. Wong EC, Buxton RB and Frank LR (1997) Implementation of quantitative perfusion imaging techniques for functional brain mapping using pulsed arterial spin labeling. NMR Biomed 10: 237-49
6. Golay X, Petersen ET and Hui F (2005) Pulsed star labeling of arterial regions (PULSAR): a robust regional perfusion technique for high field imaging. Magn Reson Med 53: 15-21
7. Luh WM, Wong EC, Bandettini PA and Hyde JS (1999) QUIPSS II with thin-slice TI1 periodic saturation: a method for improving accuracy of quantitative perfusion imaging using pulsed arterial spin labeling. Magn Reson Med 41: 1246-54
8. Lim YM, Cho YW, Shamim S, Solomon J, Birn R, Luh WM, Gaillard WD, Ritzl EK and Theodore WH (2008) Usefulness of pulsed arterial spin labeling MR imaging in mesial temporal lobe epilepsy. Epilepsy Res 82: 183-9
9. Wu WC, Mazaheri Y and Wong EC (2007) The effects of flow dispersion and cardiac pulsation in arterial spin labeling. IEEE Trans Med Imaging 26: 84-92
10. Noth U, Meadows GE, Kotajima F, Deichmann R, Corfield DR and Turner R (2006) Cerebral vascular response to hypercapnia: determination with perfusion MRI at 1.5 and 3.0 Tesla using a pulsed arterial spin labeling technique. J Magn Reson Imaging 24: 1229-35
11. Ye FQ, Frank JA, Weinberger DR and McLaughlin AC (2000) Noise reduction in 3D perfusion imaging by attenuating the static signal in arterial spin tagging (ASSIST). Magn Reson Med 44: 92-100
12. Wang J, Aguirre GK, Kimberg DY and Detre JA (2003) Empirical analyses of null-hypothesis perfusion FMRI data at 1.5 and 4 T. Neuroimage 19: 1449-62
13. Alexander ME, Baumgartner R, Summers AR, Windischberger C, Klarhoefer M, Moser E and Somorjai RL (2000) A wavelet-based method for improving signal-to-noise ratio and contrast in MR images. Magn Reson Imaging 18: 169-80

14. Nowak RD (1999) Wavelet-based Rician noise removal for magnetic resonance imaging. IEEE Trans Image Process 8: 1408-19
15. Wirestam R, Bibic A, Lätt J, Brockstedt S and Ståhlberg F (2006) Denoising of complex MRI data by wavelet-domain filtering: application to high-b-value diffusion-weighted imaging. Magn Reson Med 56: 1114-20
16. Zaroubi S and Goelman G (2000) Complex denoising of MR data via wavelet analysis: application for functional MRI. Magn Reson Imaging 18: 59-68
17. Wink AM and Roerdink JB (2004) Denoising functional MR images: a comparison of wavelet denoising and Gaussian smoothing. IEEE Trans Med Imaging 23: 374-87
18. Worsley KJ, Marrett S, Neelin P and Evans AC (1996) Searching scale space for activation in PET images. Human Brain Mapping 4: 74-90
19. Donald BP, Andrew TW and Todd O (2002) Wavelet Methods for Time Series Analysis. Journal of the American Statistical Association 97: 362-363
20. Figueiredo PM, Clare S and Jezzard P (2005) Quantitative perfusion measurements using pulsed arterial spin labeling: effects of large region-of-interest analysis. J Magn Reson Imaging 21: 676-82
21. Alexander ME, Baumgartner R, Windischberger C, Moser E and Somorjai RL (2000) Wavelet domain de-noising of time-courses in MR image sequences. Magn Reson Imaging 18: 1129-1134
22. Press WH (1992) Numerical Recipes in C: The Art of Scientific Computing (2nd edition). Cambridge University Press; 2 edition (October 30, 1992)
23. Leenders KL, Perani D, Lammertsma AA, Heather JD, Buckingham P, Healy MJ, Gibbs JM, Wise RJ, Hatazawa J, Herold S, Beaney RP, Brooks DJ, Spinks T, Rhodes C and Frackowiak RSJ. (1990) Cerebral blood flow, blood volume and oxygen utilization. Normal values and effect of age. Brain 113 (Pt 1): 27-47
24. Aguirre GK, Detre JA, Zarahn E and Alsop DC (2002) Experimental design and the relative sensitivity of BOLD and perfusion fMRI. Neuroimage 15: 488-500
25. Fernandez-Seara MA, Edlow BL, Hoang A, Wang J, Feinberg DA and Detre JA (2008) Minimizing acquisition time of arterial spin labeling at 3T. Magn Reson Med 59: 1467-71
26. Petersen ET, Lim T and Golay X (2006) Model-free arterial spin labeling quantification approach for perfusion MRI. Magn Reson Med 55: 219-32
27. Jones DK (2003) Determining and visualizing uncertainty in estimates of fiber orientation from diffusion tensor MRI. Magn Reson Med 49: 7-12

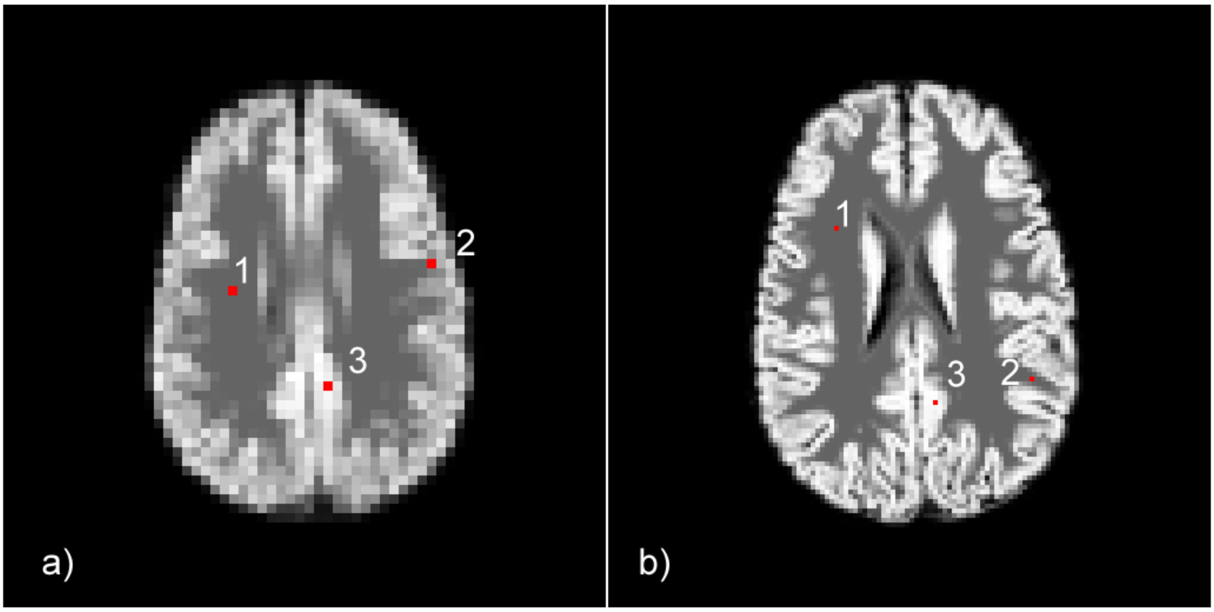

Figure 1. Synthetic, noise-free perfusion maps with voxel dimensions of (a) 3.75 × 3.75 × 6.3 mm^3 and (b) 1.875 × 1.875 × 3.6 mm^3. The assigned CBF values were 25 ml/min/100g in white matter and 65 ml/min/100g in grey matter. Partial-volume effects were considered by applying appropriate weighting factors obtained from the segmentation procedure. Detailed pixel analyses were carried out for there selected regions, i.e. for a pixel in the middle of a homogenous area (1), a pixel in the narrow groove between two sulci (2) and a pixel close to the border between grey and white matter (3). Pixel location (1) also represents the area for which the SNR was calculated before and after wavelet-domain filtering and Gaussian smoothing.

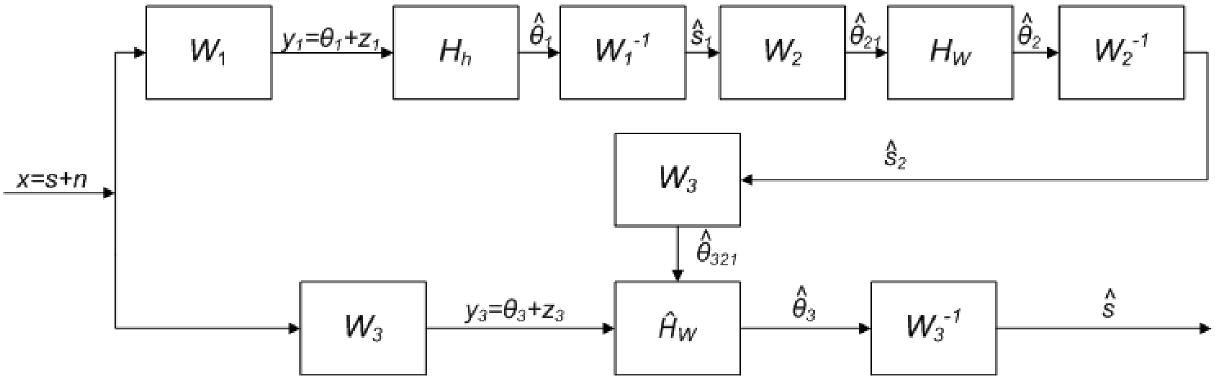

Figure 2. Block diagram of the complete wavelet-domain filtering procedure. Symbols are explained in the text.

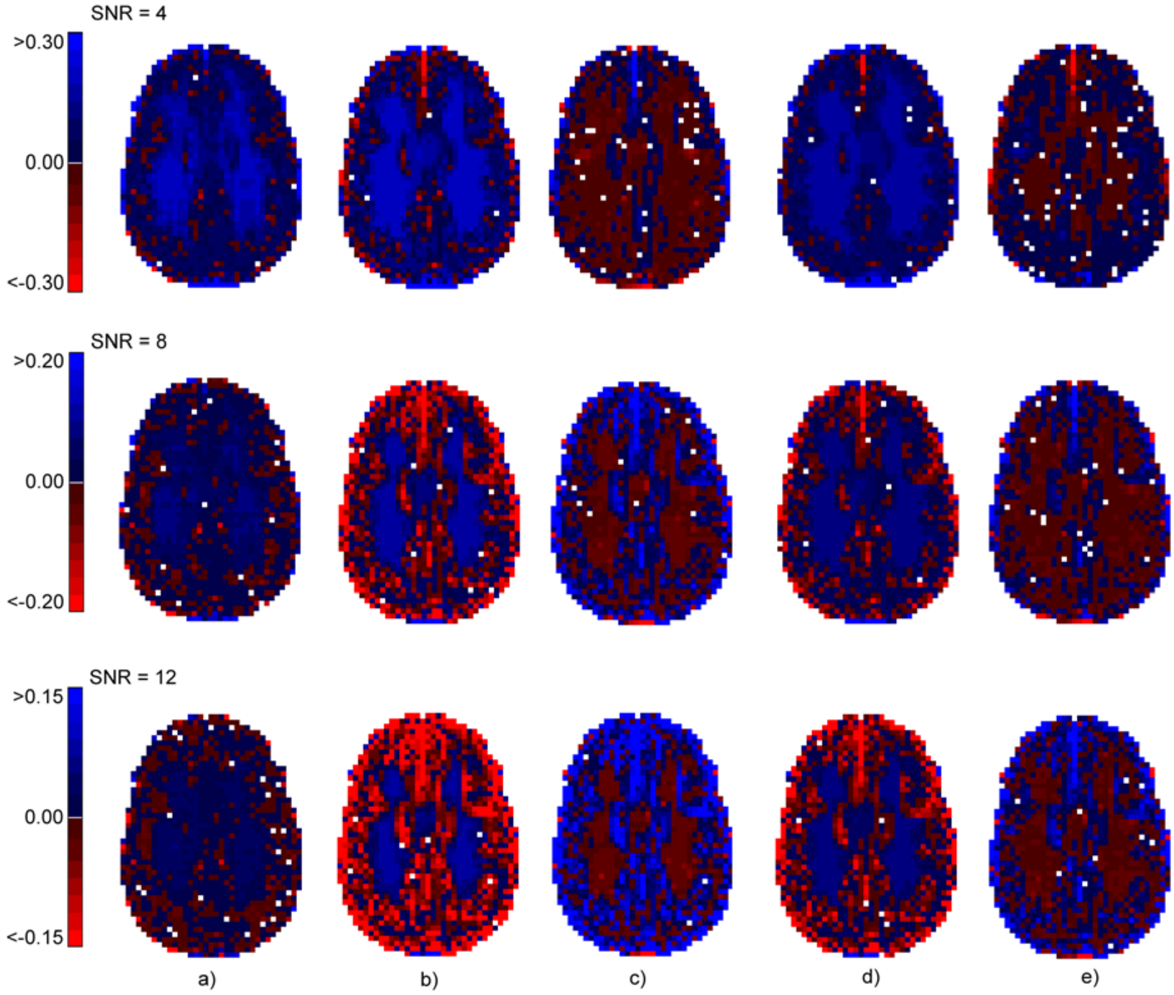

Figure 3. ΔCV maps in low-resolution simulated images. Blue/red pixels represent pixels where (a) wavelet-domain filtering and (b) Gaussian smoothing (FWHM=8 mm) were superior/inferior to non-filtering at different SNRs. Column (c) represents a direct comparison of the two filtering methods showing pixels where wavelet-domain filtering was superior to (blue) or inferior to (red) Gaussian smoothing (FWHM=8 mm) for different SNRs. Blue/red pixels in column (d) similarly show whether Gaussian smoothing (FWHM=5.6 mm) was superior/inferior to non-filtering at different SNRs and (e) again represents a direct comparison of the two methods showing pixels where wavelet-domain filtering was superior to (blue) or inferior to (red) Gaussian smoothing (FWHM=5.6 mm). The colour bars show the different levels of ΔCV and pixels in white show locations without significant difference between the means of the *CV* populations (n=100).

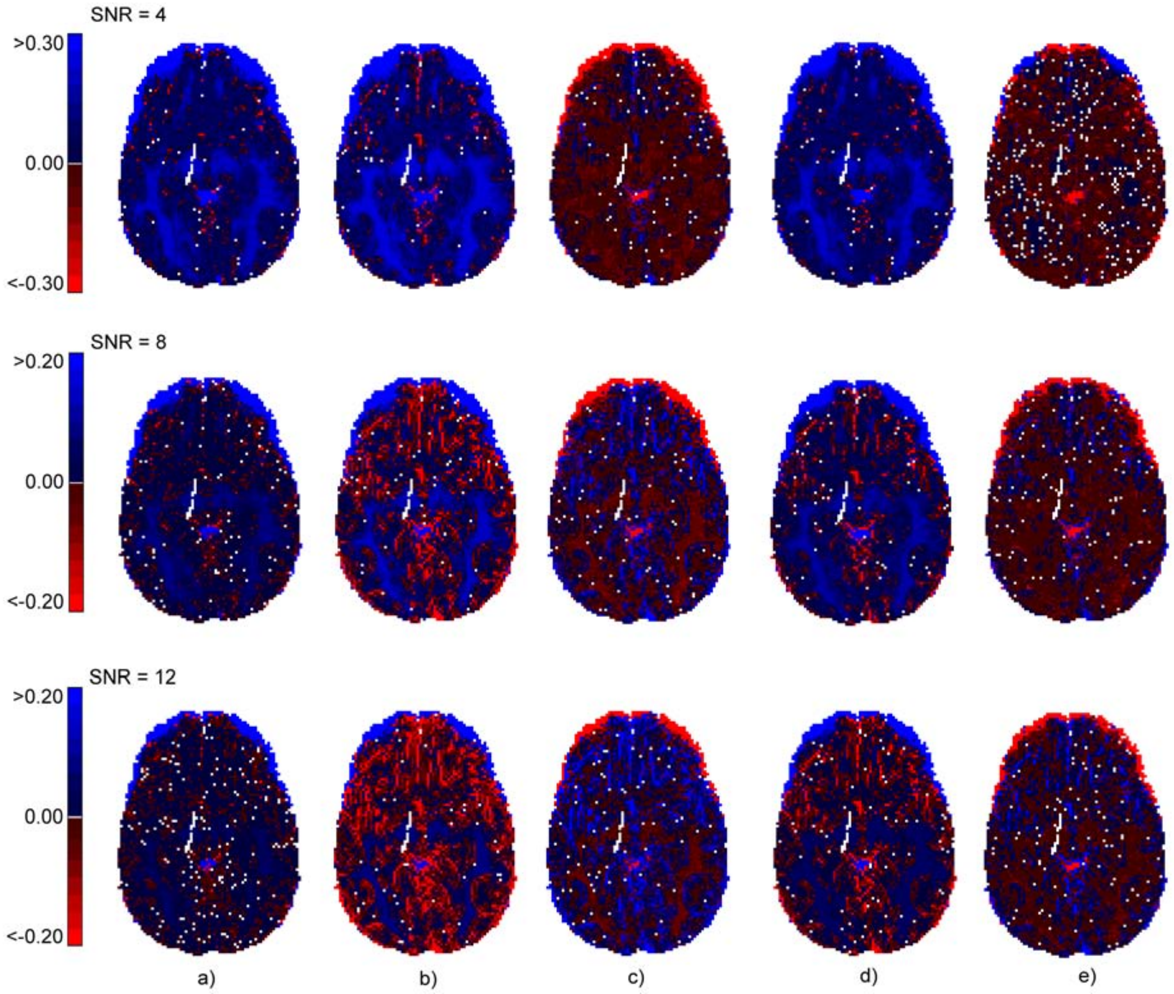

Figure 4. High-resolution simulated images. Blue/red pixels represent pixels where (a) wavelet-domain filtering and (b) Gaussian smoothing (FWHM=4 mm) were superior/inferior to non-filtering at different SNRs. Column (c) represents a direct comparison of the two filtering methods showing pixels where wavelet-domain filtering was superior to (blue) or inferior to (red) Gaussian smoothing (FWHM=8 mm) for different SNRs. Blue/red pixels in column (d) similarly show whether Gaussian smoothing (FWHM=2.8 mm) was superior/inferior to non-filtering at different SNRs and (e) again represents a direct comparison of the two methods showing pixels where wavelet-domain filtering was superior to (blue) or inferior to (red) Gaussian smoothing (FWHM=2.8 mm). The colour bars show the different levels of ΔCV and pixels in white show locations without significant difference between the means of the *CV* populations (n=100).

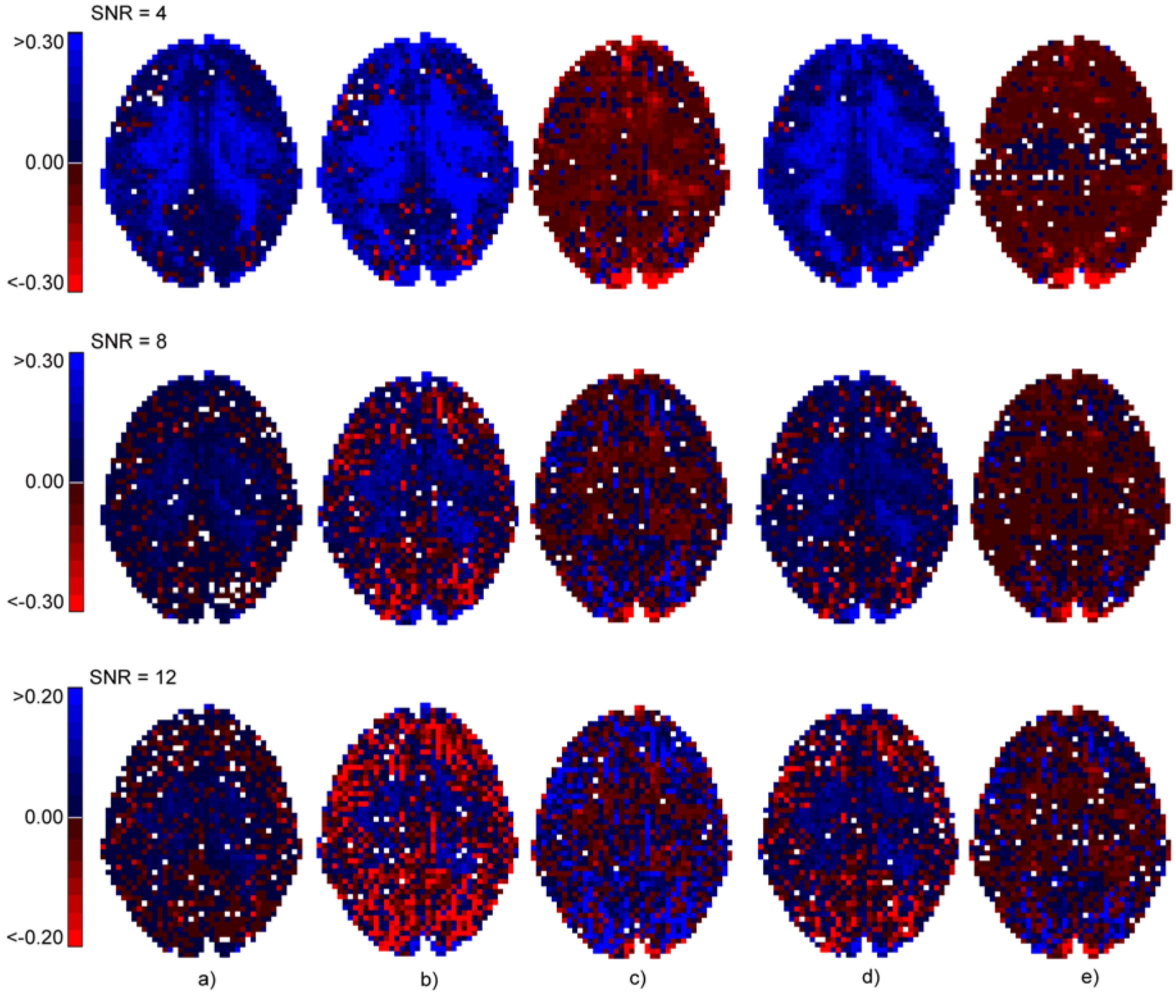

Figure 5. **ΔCV maps for the experimental images. The assignment of colours to pixels indicates where (a) wavelet-domain filtering and (b) Gaussian smoothing (FWHM=8 mm) was superior to (blue) or inferior to (red) non-filtering at different SNRs. Column (c) represents a direct comparison of the two methods showing pixels where wavelet-domain filtering was superior to (blue) or inferior to (red) Gaussian smoothing (FWHM=8 mm) for different SNRs. Column (d) shows pixels where Gaussian smoothing (FWHM=5.6 mm) was superior to (blue) or inferior to (red) non-filtering at different SNRs and column (e) represents a direct comparison of the two methods showing pixels where wavelet-domain filtering was superior to (blue) or inferior to (red) Gaussian smoothing (FWHM=5.6 mm). The colour bars show the different levels of ΔCV and pixels in white show locations without significant difference between the means of the *CV* populations (n=100)..**

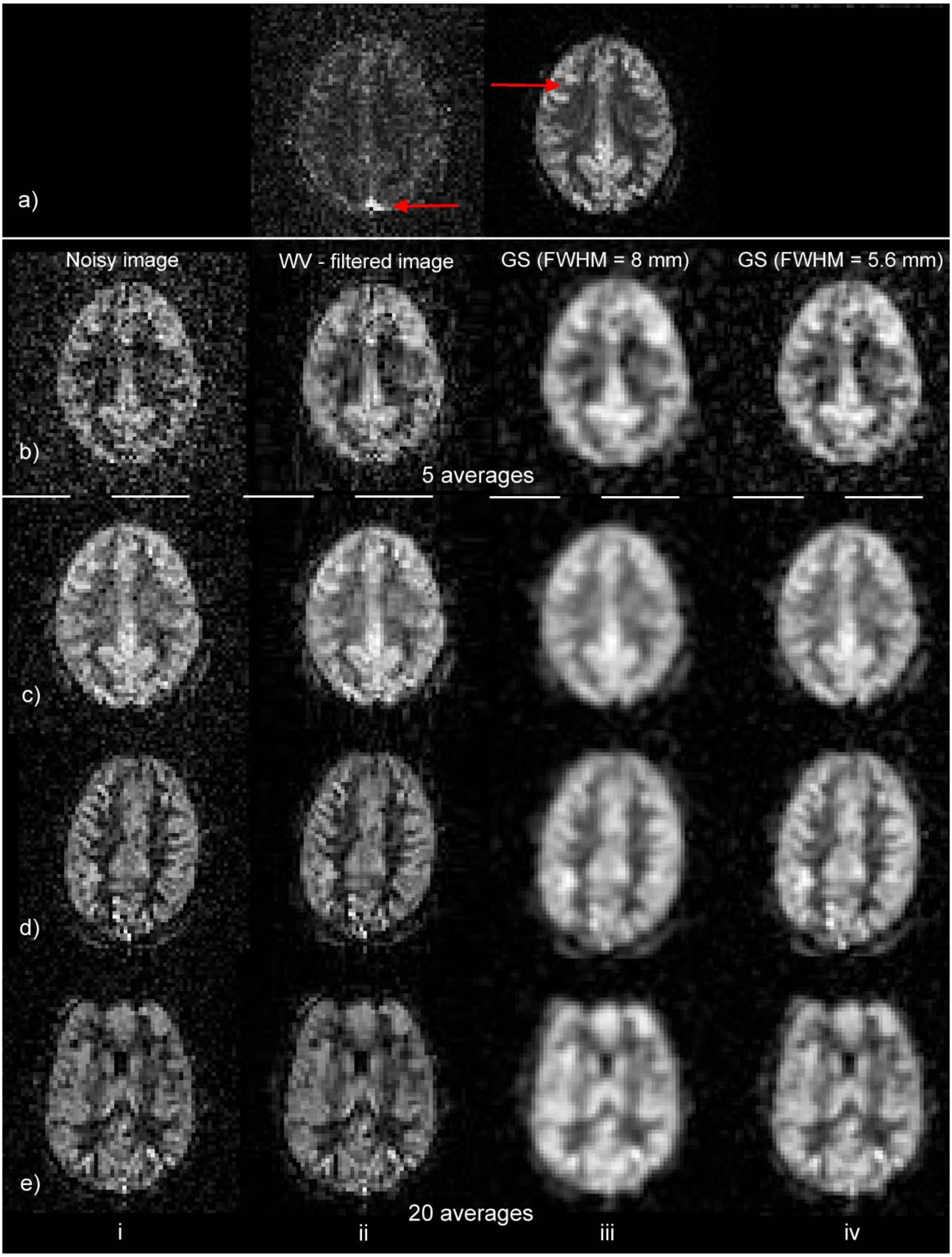

Figure 6. (a) To the left is an original, non-averaged difference image from volunteer #1 (also illustrating an artefact in the sagittal-sinus region). To the right is a reference image from volunteer #1 computed from 300 experimental difference images. The arrow indicates the pixel location for which the CBF was analysed before and after noise reduction (cf. Figure 7d). (b) Column (i) shows non-filtered image computed from 5 experimental difference images (SNR=4) from volunteer #1, (ii) the corresponding

wavelet (WV) filtered image, (iii) the corresponding Gaussian smoothed image (FWHM=8 mm) and (iv) the corresponding Gaussian smoothed image (FWHM=5.6 mm). (c) Similar arrangement as in (b) but with the non-filtered image from volunteer #1 calculated from 20 averages (SNR=8), (d) as in (c) but data obtained from volunteer #2 and (e) as in (c) but data obtained from volunteer #3.

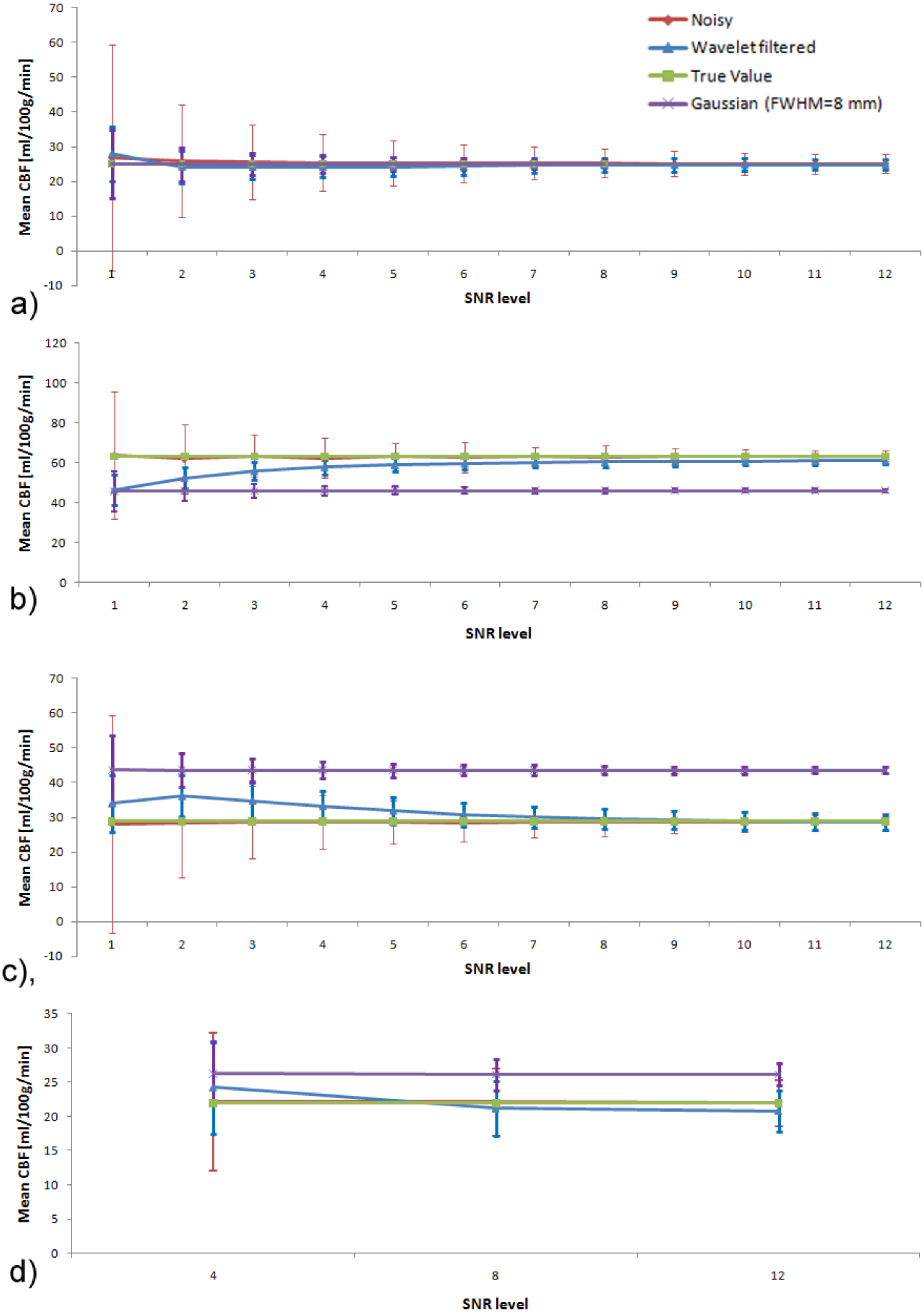

Figure 7. Mean CBF values for original non-filtered images, wavelet filtered and Gaussian smoothed images, at different SNR levels, with error bars corresponding to ±1 SD: (a) Pixel in simulated WM in the

centre of an apparently homogenous area, (b) Pixel in simulated GM in the vicinity of the borderline between WM and GM (the selected pixel was located between two sulci). (c) Pixel in simulated WM in the vicinity of the borderline between WM and GM (the selected pixel was located between two sulci). (d) Pixel located between two sulci in experimental image (see Figure 6a). The green lines represents the true value.

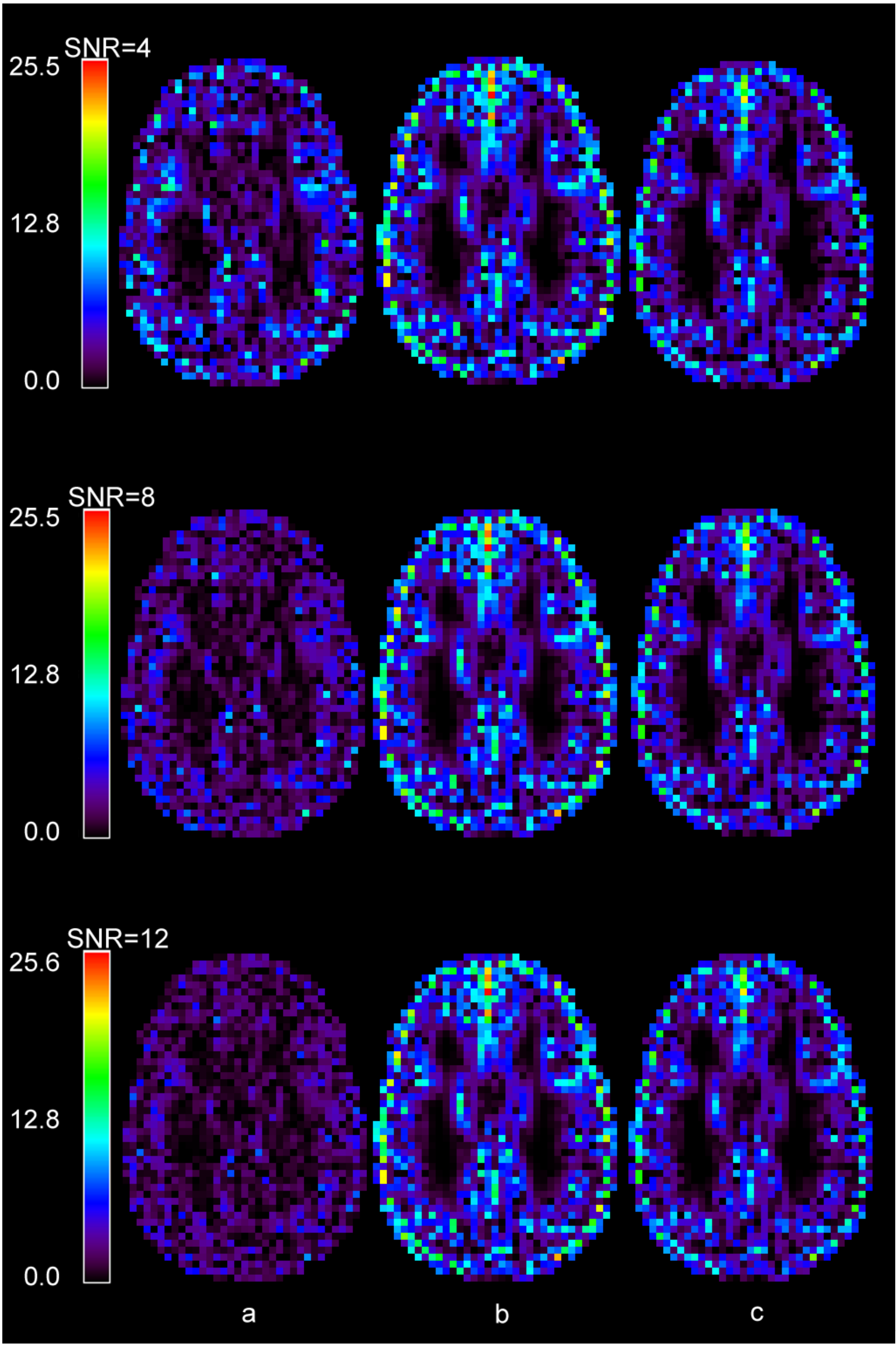

Figure 8. Simulated data: Bias in (a) wavelet-filtered images, (b) Gaussian smoothed images (FWHM=8 mm)

and (c) Gaussian smoothed images (FWHM=5.6 mm) for different SNR levels. Pixels with no significant bias are shown in black.

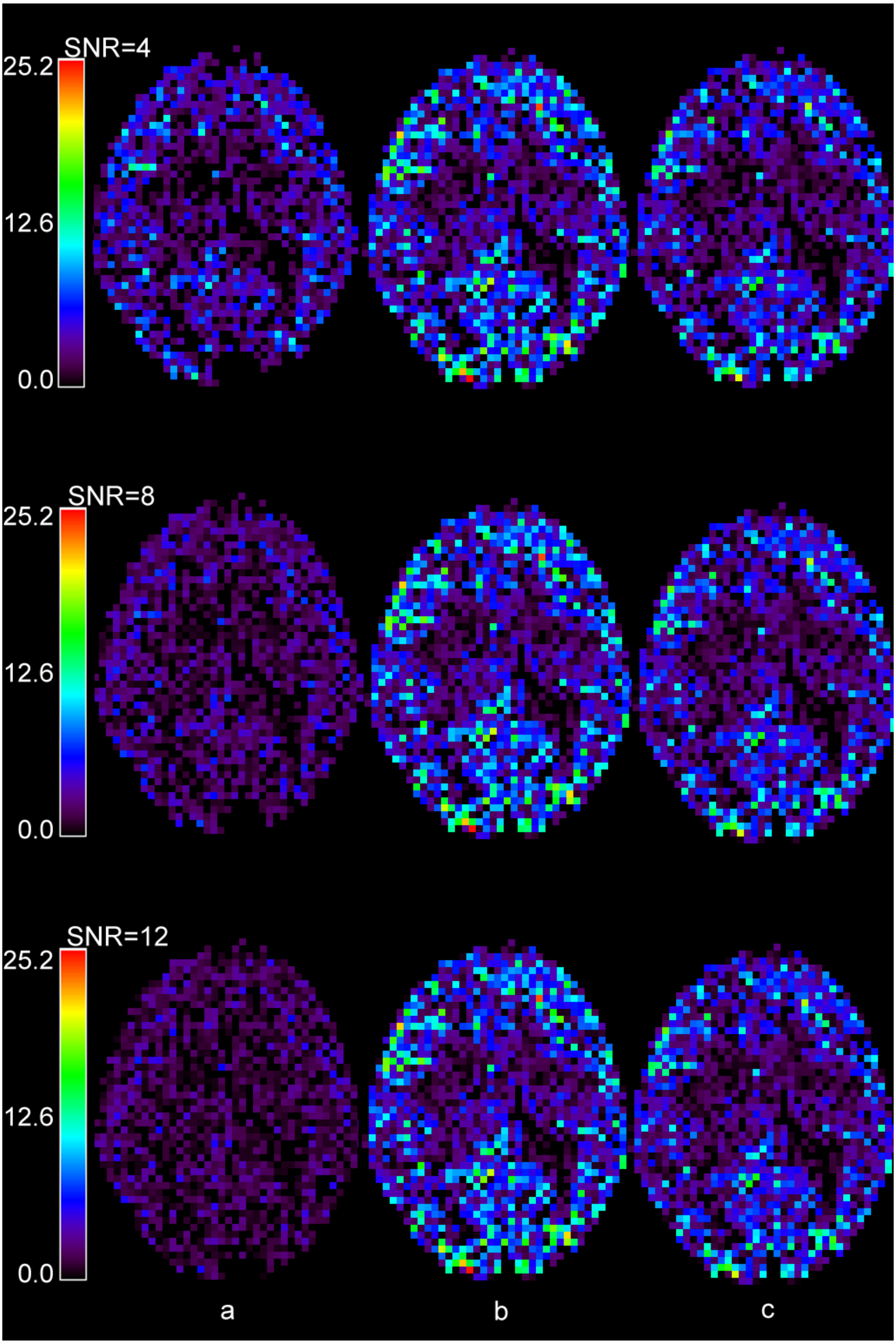

Figure 9. Experimental data: Bias in (a) wavelet-filtered images, (b) Gaussian smoothed images

(FWHM=8 mm) and (c) Gaussian smoothed images (FWHM=5.6 mm) for different SNR levels. Pixels with no significant bias are shown in black.

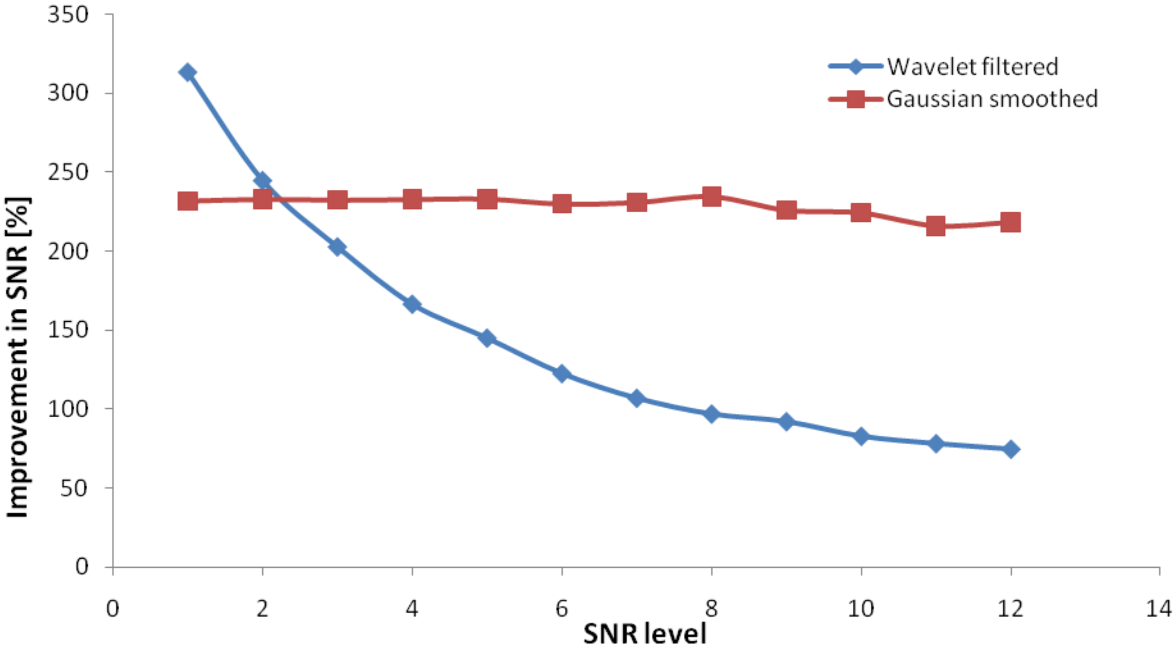

Figure 10. The filtering-induced improvement in SNR as a function of SNR for simulated images, achieved by wavelet-domain filtering and Gaussian smoothing (FWHM=8 mm). Data correspond to pixel location (1) in Fig. 1.